

www.acsabm.org Forum Article

Ratiometric Fluorogenic RNA-Based Sensors for Imaging Live-Cell Dynamics of Small Molecules

Rigumula Wu, Aruni P.K.K. Karunanayake Mudiyanselage, Kewei Ren, Zhining Sun, Qian Tian, Bin Zhao, Yousef Bagheri, David Lutati, Puspam Keshri, and Mingxu You*



Cite This: ACS Appl. Bio Mater. 2020, 3, 2633–2642



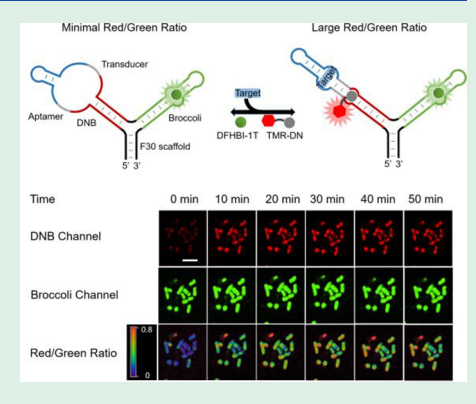
ACCESS

Metrics & More

Article Recommendations

s Supporting Information

ABSTRACT: Imaging the cellular dynamics of metabolites and signaling molecules is critical for understanding various metabolism and signal transduction pathways. Genetically encoded RNA-based sensors are emerging powerful tools for this purpose. However, it was challenging to use these sensors to precisely determine the intracellular concentrations of target analytes. To solve this problem, we have recently developed ratiometric sensors using an orthogonal pair of RNA/fluorophore conjugates: Broccoli/DFHBI-1T (3,5-difluoro-4-hydroxybenzylidene-1-trifluoroethylimidazolinone) and DNB (dinitroaniline-binding aptamer)/SR-DN (sulforhodamine B-dinitroaniline). The cellular DNB-to-Broccoli fluorescence intensity ratio can be directly applied to quantify the target concentrations at the single-cell level. Unfortunately, due to the instability of the SR-DN dye, this ratiometric sensor is difficult to use for monitoring target dynamics. Herein, by replacing SR-DN with a stable TMR (tetramethylrhodamine)-DN dye, we developed a ratiometric sensor



system based on Broccoli/DFHBI-1T and DNB/TMR-DN, which can be used for dynamic imaging in living cells. We believe these advanced genetically encoded ratiometric sensors can be widely used for intracellular studies of various target analytes.

KEYWORDS: aptamer, biosensors, cellular imaging, fluorogenic RNA, ratiometric sensors

■ INTRODUCTION

Direct in situ detection of metabolites and signaling molecules is crucial for understanding various cellular functions and their molecular mechanisms. Fluorescent probes are particularly useful tools for this purpose. 1-4 These probes can be used to image the dynamics and distributions of various target analytes in living cells. For example, several fluorescent protein (FP) based genetically encoded sensors have been developed. 5,6 Unlike synthetic fluorescent probes, these genetically encoded sensors can be directly expressed intracellularly and have low toxicity to cells. A protein- or peptide-based target-binding domain is normally required for the function of these FP-based sensors. These domains should specifically bind with the target analytes and meanwhile undergo a large conformational change upon the target binding.^{7,8} Unfortunately, the number of available target-binding domains is still limited. Moreover, the poor sensitivity and detection range further hinder the wide applications of these FP sensors for many target analytes. 9,10

We and others have developed another type of genetically encoded sensor based on fluorogenic RNA aptamers. These RNA-based sensors have been applied for the live-cell imaging of various RNAs, proteins, small molecules, and metal ions. RNA aptamers are short single-stranded ribonucleic acids that can fold into specific structures and bind the target analytes with high specificity and affinity. 21,222

Fluorogenic RNA aptamers, such as Spinach or Broccoli, can bind and activate the fluorescence of cell membrane permeable dyes, such as 3,5-difluoro-4-hydroxybenzylidene-1-trifluoro-ethyl-imidazolinone (DFHBI-1T).^{23,24} DFHBI-1T exhibits undetectable fluorescence by itself, but a much higher fluorescence signal is achieved upon binding with Spinach or Broccoli.

Most fluorogenic RNA-based sensors to date are developed based on imaging signals from a single channel. However, considering the cellular variations in the RNA expression and degradation levels, these single-channel sensors are difficult for the accurate quantification of the cellular concentrations and distributions of target analytes. To solve this problem, we have recently developed a type of ratiometric RNA-based sensors using an orthogonal pair of RNA/fluorophore conjugates, Broccoli/DFHBI-1T ($\lambda_{\rm ex}/\lambda_{\rm em}$, ~480/503 nm) and DNB/SR-DN ($\lambda_{\rm ex}/\lambda_{\rm em}$, ~571/591 nm). The DNB aptamer can specifically bind with a quencher moiety, dinitroaniline (DN). DN is an efficient contact quencher for a variety of

Special Issue: Nucleic Acids: Chemistry, Nanotechnology, and Bioapplications

Received: December 30, 2019 Accepted: February 7, 2020 Published: February 19, 2020





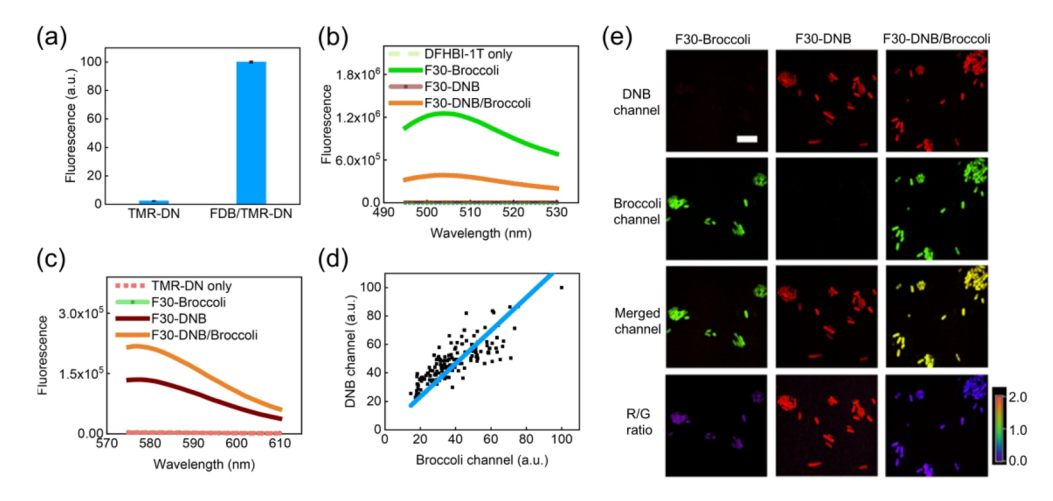


Figure 1. (a) Fluorescence of TMR-DN recovered by the addition of F30-DNB/Broccoli (FDB). *In vitro* fluorescence assay was conducted using 0.5 μM of TMR-DN in the presence or absence of 10 μM of F30-DNB/Broccoli. (b, c) Fluorescence spectra as measured with 20 μM DFHBI-1T, 10 μM TMR-DN, and 10 μM each RNA construct by exciting at 480 (b) or 555 nm (c). (d) Linear correlation observed between DNB and Broccoli fluorescence in ~150 individual cells expressing F30-DNB/Broccoli. Pearson's $r^2 = 0.95$. (e) Fluorescence imaging of BL21 (DE3)* cells expressing F30-Broccoli, F30-DNB, or F30-DNB/Broccoli in the presence of 200 μM DFHBI-1T and 0.5 μM TMR-DN. DNB-to-Broccoli (R/G) ratiometric images were shown as well. Scale bar, 10 μm.

fluorophores such as sulforhodamine B (SR) and tetramethylrhodamine (TMR).²⁶ By chemically conjugating SR with DN, the formed SR-DN conjugate exhibits efficient fluorescence quenching. Meanwhile, the physical separation of SR and DN through binding with the DNB aptamer could effectively recover the SR fluorescence (Figures S1 and S2).²⁶

In our previous study, we demonstrated the use of Broccoli/DFHBI-1T and DNB/SR-DN-based ratiometric sensors to quantify the intracellular concentrations and distributions of target analytes. However, we realized that this sensor system may not be suitable for real-time monitoring of the dynamic changes of target cellular levels. The fluorescence intensity of the DNB/SR-DN complex somehow decreased over time, while the Broccoli/DFHBI-1T signal was quite stable within the same time period (Figure S3). As a result, it is difficult to distinguish fluorescence signal change induced by the target analytes from that by the intrinsic instabilities of DNB/SR-DN. An orthogonal pair of chemically and photophysically stable RNA/fluorophore complexes are thus still needed for imaging and quantifying the cellular dynamics of target analytes.

Here, we demonstrated that by simply replacing SR-DN with TMR-DN, a stable Broccoli/DFHBI-1T and DNB/TMR-DN-based ratiometric sensor system can be used to quantify the cellular distributions and monitor the dynamics of target small molecules. We believe these novel genetically encoded sensors can be widely applied for the live-cell imaging and quantification of various cellular targets.

■ EXPERIMENTAL SECTION

Reagents. All the chemicals were purchased from Sigma or Fisher Scientific unless otherwise noted. C-di-GMP, c-di-AMP, and cGAMP were ordered from Axxora, LLC. Commercial reagents were used without further purification. All the DNA oligonucleotides were synthesized by W. M. Keck Oligonucleotide Synthesis Facility (Yale University School of Medicine) or Integrated DNA Technologies (Coralville, IA).

Instrumentation. Double-stranded DNA strands for *in vitro* transcription were prepared by PCR amplification using an Eppendorf Mastercycler. NanoDrop One UV—vis spectrophotometer was used to quantify the concentration of nucleic acids. All the *in vitro* fluorescence tests were conducted with a PTI fluorimeter (Horiba,

New Jersey, NJ). All the intracellular images were taken by a Yokogawa spinning disk confocal on a Nikon Eclipse-TI inverted microscope.

Synthesis of the Tetramethylrhodamine-PEG₃-Dinitroaniline (TMR-DN) Conjugate. TMR-DN was synthesized following a previously reported procedure. 26 Briefly, a 100 μ L DMF solution of DN-PEG3-amine (3.6 mg, 11.4 μ mol) was added to a 100 μ L DMF solution of 5-carboxy tetramethylrhodamine N-succinimidyl ester (2.0 mg, 3.8 μ mol). The reaction mixture was stirred at room temperature for 30 min. The reaction mixture was purified through a reversed-phase C18 column (60% acetonitrile, 0.1% trifluoracetic acid) and yielded TMR-DN (1.5 mg, 55% yield) (Figure S4a). High-resolution ESI (positive): calculated 727.2722, found 727.5 for $C_{37}H_{39}N_6O_{10}$ (Figure S4b).

In Vitro Transcription of the RNA Sensors. All the purchased DNA oligonucleotides were dissolved in 10 mM Tris-HCl, 0.1 mM EDTA at pH= 7.5 and stored at −20 °C. A Phusion high-fidelity DNA polymerase (Thermo Fisher, Waltham, MA) was used to perform PCR reactions in an Eppendorf Mastercycler. The PCR product was purified by a QIAquick PCR purification kit (Qiagen, Germantown, MD). All the RNAs were transcribed using a HiScribe T7 high yield RNA synthesis kit (New England BioLabs, Ipswich, MA) and were treated with DNase I (RNase-free) (New England BioLabs) to remove the DNA fragments and then were column-purified. The final RNA products were further validated in 10% denaturing polyacrylamide gels.

Fluorescence Assays. The *in vitro* transcribed RNAs and target analytes were incubated in a buffer consisting of 40 mM Tris, 5 mM MgCl₂, and 100 mM KCl at pH = 7.6 prior to the fluorescence detection. For the green channel (Broccoli), emission spectra of 495–530 nm were collected by exciting at 480 nm. For the red channel (DNB), emission spectra of 585–620 nm or 575–610 nm were collected by exciting at 571 nm (SR-DN) or 555 nm (TMR-DN), respectively. All the data were plotted and analyzed using an Origin software.

Cellular Imaging and Data Analysis. The construction of vectors used in this study has been described previously. ^{2.5} Cellular imaging was conducted based on a previously established protocol. ²⁷ Briefly, BL21 (DE3)* *E. coli* cells were grown in LB media at 37 °C, 200 rpm until the optical density at 600 nm reaching 0.4–0.5 and then 1 mM isopropyl β-D-1-thiogalactopyranoside (IPTG) was added to induce the T7 RNA polymerase synthesis for 1–3 h. Cells were then pelleted and resuspended in a DPBS buffer followed by attaching on a glass surface pretreated with poly-L-lysine. The Broccoli channel,

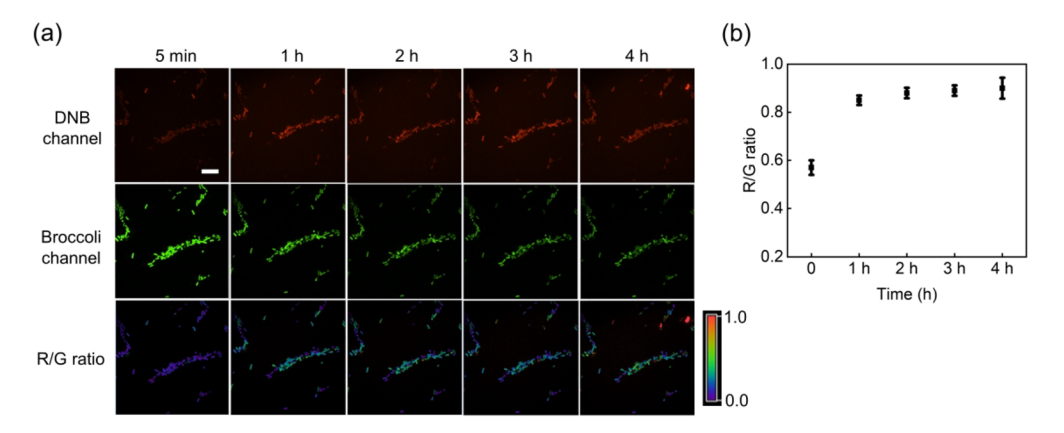


Figure 2. (a) Confocal fluorescence imaging of *E. coli* cells expressing F30-DNB/Broccoli after the addition of 200 μ M DFHBI-1T and 0.1 μ M TMR-DN. The Broccoli channel (green), DNB channel (red), and ratiometric images were shown. After 1 h incubation, some fluorescence signal decrease in both DNB and Broccoli channels were likely due to the RNA degradation. Scale bar: 10 μ m. (b) We analyzed 250 cells from three experimental replicates at each time point as that shown in panel a. The DNB-to-Broccoli fluorescence ratio (R/G) remained at the same level within the 4 h imaging time. Shown are mean and SEM values.

DNB sensor channel, and Sytox Blue channel were excited with 488, 561, and 405 nm lasers, respectively, through a 100× oil immersion objective. Data analysis was performed with a NiS-Elements AR Analysis software and an ImageJ software. Data calculation and fitting was done using an Origin software.

RESULTS AND DISCUSSION

Orthogonal DNB/TMR-DN and Broccoli/DFHBI-1T Conjugates for Potential Ratiometric Imaging. Based on some previous reports, ^{26,28} the TMR dye can be efficiently quenched by the conjugated DN and the further binding of a DNB aptamer to DN will recover the fluorescence of TMR. We asked if the DNB/TMR-DN conjugate can be used for developing ratiometric sensors. We first synthesized a TMR-DN conjugate following a previously established protocol.²⁶ To test if TMR-DN can be directly used in our previously developed RNA sensor constructs, we in vitro transcribed an F30-DNB/Broccoli RNA strand (Table S1). This strand contains both a DNB aptamer and a Broccoli aptamer, which are linked by an F30 scaffold. After incubating F30-DNB/Broccoli with TMR-DN, a 42.3-fold fluorescence activation was observed (Figure 1a). Importantly, such a fluorescence signal was quite stable. For example, during a 1.5 h observation time, the RNA/TMR-DN conjugate exhibited almost no fluorescence decrease (Figure S3b), while at the same time, the fluorescence signal of SR-DN-based conjugate was quenched by ~70% (Figure S3a). The DNB/TMR-DN conjugate could be potentially a better choice than DNB/SR-DN for monitoring the dynamic variations of target analytes.

We next asked if the Broccoli/DFHBI-1T ($\lambda_{\rm ex}/\lambda_{\rm em}$, 480/503 nm) and DNB/TMR-DN ($\lambda_{\rm ex}/\lambda_{\rm em}$, 555/582 nm) conjugates can be used as an orthogonal fluorescent pair. Such orthogonality, i.e., the fluorescence signals of two RNA/fluorophore conjugates do not affect each other, is critical for the ratiometric quantification. Here, we prepared another two RNA strands containing either a DNB (F30-DNB) or a Broccoli aptamer (F30-Broccoli) within an F30 scaffold (Table S1). Interestingly, some Förster resonance energy transfer (FRET) may occur between Broccoli/DFHBI-1T and DNB/TMR-DN (Figure 1b and c). Nevertheless, these two RNA/fluorophore conjugates can still provide orthogonal fluorescent signals for the potential development of ratiometric sensors. In the presence of both DFHBI-1T and TMR-DN, the Broccoli/

DFHBI-1T and DNB/TMR-DN fluorescence could be clearly distinguished from each other, while the DNB/DFHBI-1T and Broccoli/TMR-DN conjugate exhibited minimal fluorescence.

We next wanted to see if DNB/TMR-DN and Broccoli/ DFHBI-1T can be orthogonally imaged in the living cells. To test this, we constructed three plasmids expressing either only one type of fluorogenic RNA (F30-Broccoli and F30-DNB) or both aptamers (F30-DNB/Broccoli). After transforming into BL21 (DE3)* E. coli cells, the expression of fluorogenic RNAs was induced by adding 1 mM isopropyl β -D-1-thiogalactopyranoside (IPTG). After 3 h IPTG induction, in the presence of both DFHBI-1T and TMR-DN, the cellular fluorescence was determined using a spinning disk confocal fluorescence microscope. As shown in Figure 1e, the Broccoli and DNB fluorescence could be clearly visualized in two separate imaging channels. The fluorescence activation of both Broccoli/ DFHBI-1T and DNB/TMR-DN complex was not influenced by the existence of the other RNA/fluorophore complex in the cells. DNB/TMR-DN and Broccoli/DFHBI-1T can function as an orthogonal fluorescent pair for live-cell imaging.

Using F30-DNB/Broccoli-expressing *E. coli* cells, we further quantified the correlations between the cellular fluorescence of DNB/TMR-DN and Broccoli/DFHBI-1T. After analyzing ~150 individual cells, a linear correlation was observed between two imaging channels (Figure 1d). In addition, the cellular fluorescence signals of both RNA/fluorophore conjugates were linearly correlated with the RNA expression levels (Figure S5). After subtracting the cellular background, the DNB-to-Broccoli fluorescence ratio is independent of the cellular RNA expression levels. Even though there are obvious cell-to-cell variations in the RNA expression levels (Figure 1d), we can use either Broccoli or DNB fluorescence to determine the RNA aptamer concentrations in each individual cell. As a result, the DNB/TMR-DN and Broccoli/DFHBI-1T conjugate pair can be used for cellular quantifications.

We next tested if this conjugate pair can be applied for the kinetic measurement using these F30-DNB/Broccoli-expressing BL21 (DE3)* *E. coli* cells. After adding TMR-DN and DFHBI-1T, the fluorescence signals from both DNB and Broccoli imaging channels were monitored for 4 h (Figure 2a). During this period of time, both DNB/TMR-DN and Broccoli/DFHBI-1T fluorescence were maintained at high levels. Even though the fluorescence signals from both

ACS Applied Bio Materials

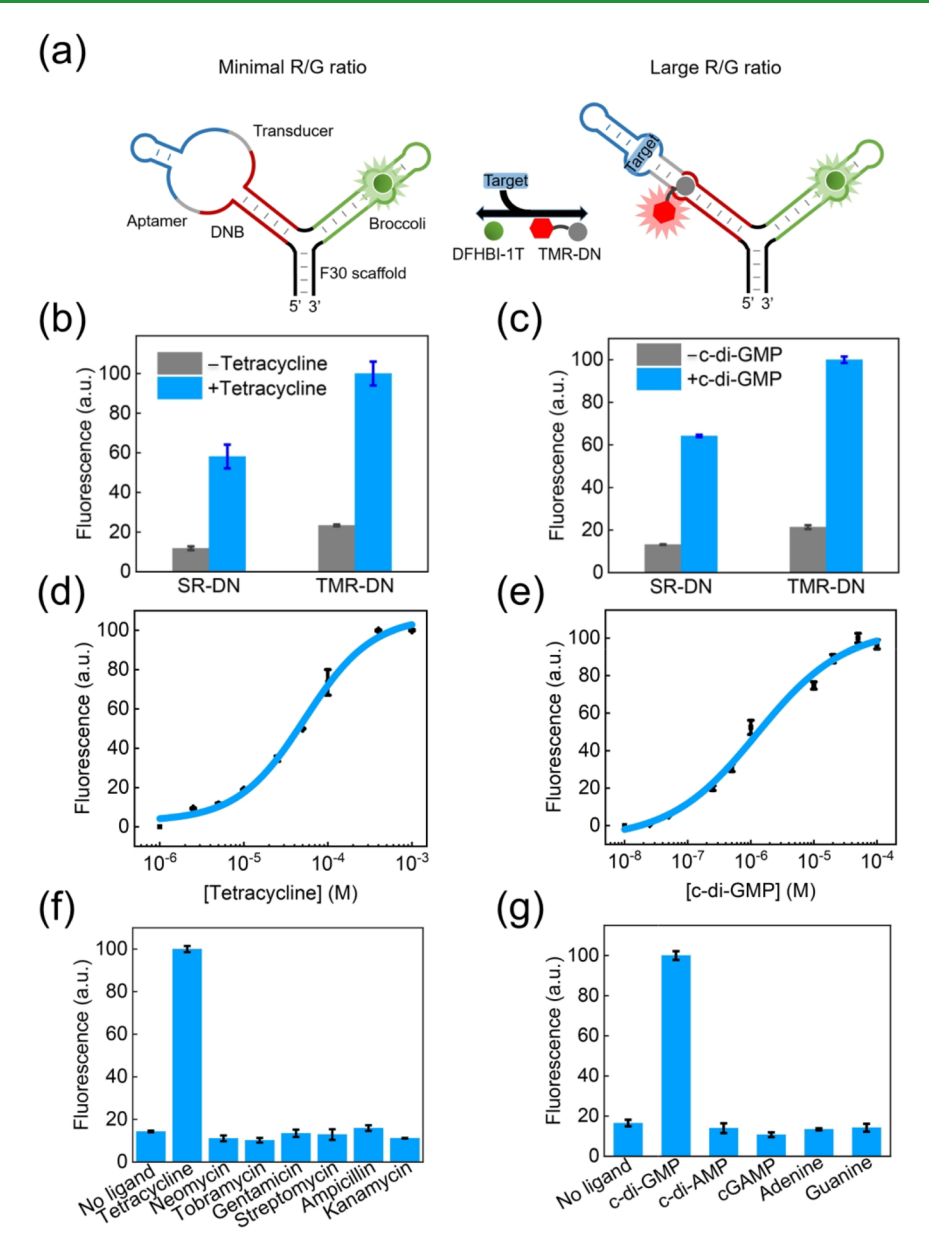


Figure 3. (a) Schematic of the ratiometric sensor that comprises an F30 scaffold (black), a Broccoli (green), and a DNB-based sensor. The DNB-based sensor is composed of a DNB (red), a target-binding aptamer (blue) and a transducer (gray). Target binding to the aptamer (blue) stabilizes the transducer, enabling DNB to fold and activate the fluorescence of TMR-DN. (b) *In vitro* fluorescence test with tetracycline-targeting ratiometric sensor using SR-DN ($\lambda_{ex}/\lambda_{em}$, ~571/591 nm) or TMR-DN ($\lambda_{ex}/\lambda_{em}$, ~555/582 nm). The fluorescence was measured with 5 μM RNA and 0.5 μM SR-DN or TMR-DN in the presence or absence of 500 μM tetracycline. (c) *In vitro* fluorescence test with c-di-GMP targeting ratiometric sensor. The fluorescence was measured with 5 μM RNA and 0.5 μM SR-DN or TMR-DN in the presence of 10 μM c-di-GMP. (d, e) Dose—response curves for the detection of tetracycline (d) or c-di-GMP (e) by the ratiometric sensor. (f) Selectivity of the tetracycline-targeting ratiometric sensor. The fluorescence intensity was measured in a solution containing 2.5 μM RNA, 20 μM DFHBI-1T, and 0.5 μM TMR-DN in the presence of 400 μM tetracycline or analog. (g) Selectivity of the c-di-GMP-targeting ratiometric sensor. The fluorescence intensity was measured in a solution containing 2.5 μM RNA, 20 μM DFHBI-1T, and 0.5 μM TMR-DN in the presence of 50 μM c-di-GMP or analog. Shown are mean and SEM values of three independent replicates.

channels were decreased after 1 h, the DNB-to-Broccoli fluorescence ratio remained constant (Figure 2). As a result, such decrease in the cellular fluorescence was due to the RNA degradation, rather than the instability of the DNB/TMR-DN conjugate. This result is quite different from that observed with the unstable DNB/SR-DN conjugate (Figure S3c). By replacing SR-DN with TMR-DN, the orthogonal and stable DNB/TMR-DN and Broccoli/DFHBI-1T conjugate pair can be used for kinetic imaging in the living cells.

Design and *In Vitro* **Characterization of RNA-Based Ratiometric Sensors.** To develop TMR-DN-based ratiometric sensors for detecting target analytes, we wondered if we could directly use our previously optimized F30-DNB/Broccoli-based RNA strands (Table S1). In this sensor construct, a target-binding aptamer was fused into DNB through a transducer domain (Figure 3a). The binding of target analytes will induce the folding of DNB and activate the TMR-DN fluorescence. Broccoli was used as a reference to normalize the cellular expression levels of the RNA sensors. As

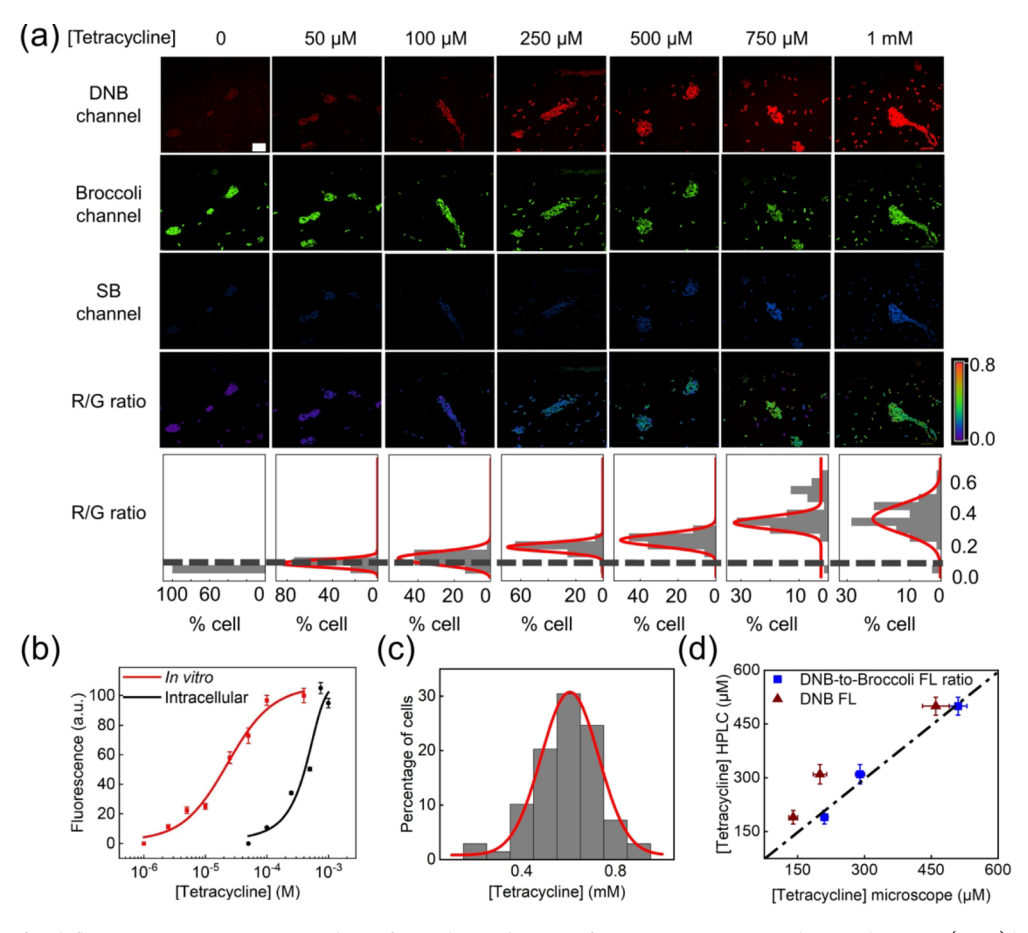


Figure 4. (a) Confocal fluorescence imaging was taken after 2 h incubation of $0-1000~\mu\mathrm{M}$ tetracycline with BL21 (DE3)* cells that express tetracycline-targeting ratiometric sensor. Here, $200~\mu\mathrm{M}$ DFHBI-1T, $0.5~\mu\mathrm{M}$ TMR-DN, and $1.5~\mu\mathrm{M}$ Sytox blue (SB) was added. The tetracycline-targeting DNB sensor channel (red), Broccoli channel (green), SB channel (blue), and DNB-to-Broccoli (R/G) ratiometric image were shown. Scale bar, $10~\mu\mathrm{m}$. According to the R/G ratio of 210 individual cells from three experimental replicates, cellular distribution curves were generated. (b) *In vitro* (red) and intracellular (black) dose–response curves of tetracycline sensor based on the mean and SEM of the DNB-to-Broccoli fluorescence ratio. (c) Distributions of intracellular tetracycline amounts after adding 1 mM tetracycline in the solution. Individual cells were binned according to their tetracycline concentrations. The percentage of cells in each bin was plotted. (d) Validation of the determined cellular tetracycline levels based on either DNB fluorescence only or DNB-to-Broccoli fluorescence ratio with an HPLC assay after adding 250, 500, or $1000~\mu\mathrm{M}$ tetracycline.

a result, the DNB-to-Broccoli fluorescence ratio can be used to quantify target concentrations.

To test this idea, we prepared two F30-DNB/Broccoli-based RNA sensors targeting tetracycline and c-di-GMP, respectively. ^{25,29,30} After the *in vitro* transcription of these RNA sensors, we first detected the target-induced fluorescence signals. A similar level of fluorescence enhancement was observed using either TMR-DN or SR-DN for the detection of both tetracycline (4.3-fold vs 4.9-fold) and c-di-GMP (4.7-fold vs 4.9-fold) (Figure 3b and 3c). In addition, no difference in the Broccoli fluorescence was observed after adding these targets (Figure S6a and b). Indeed, by simply replacing the SR-DN with TMR-DN, we can directly apply the previously developed RNA sensor strands to detect target analytes.

We next wanted to know if these sensors could still detect the targets within the physiological concentration range. Dose—response curves were generated by adding different amounts of tetracycline or c-di-GMP into a solution containing 5 μ M RNA sensor, 20 μ M DFHBI-1T, and 0.5 μ M TMR-DN (Figure 3d and e). Under this condition, the half-maximal fluorescence was reached after adding 1.3 μ M c-di-GMP or 53 μ M tetracycline. If we defined the dynamic range as the target concentration that induced 10%—90% of maximum fluores-

cence, a moderate dynamic range was observed, $0.1-20~\mu\mathrm{M}$ for c-di-GMP and $2.5-131~\mu\mathrm{M}$ for tetracycline. Indeed, this TMR-DN-based sensor system can be potentially used to detect c-di-GMP in their physiological concentration range ($\sim 0.05-10~\mu\mathrm{M}$). For bacterial cells, the minimum inhibitory concentration of tetracycline is $\sim 300~\mu\mathrm{M}$. Considering that the intracellular level of antibiotics is normally lower than that added outside of the cells, the developed TMR-DN-based tetracycline sensor could also be suitable for potential antibacterial studies.

We also confirmed the selectivity of these sensors toward their target analytes. As expected, the fluorescence signal of the tetracycline-targeting sensor was not activated by other antibiotics such as tobramycin, gentamicin, neomycin, kanamycin, ampicillin, or streptomycin (Figure 3f). Similarly, the c-di-GMP-targeting sensor maintained good selectivity toward its target among analogs including c-di-AMP, cGAMP, adenine, and guanine (Figure 3g). All these *in vitro* results indicated that TMR-DN-based sensors can be used to selectively detect their target analytes within the physiological cellular concentrations.

Ratiometric Imaging and Quantification in Living Cells. We next asked if we could use these ratiometric sensors

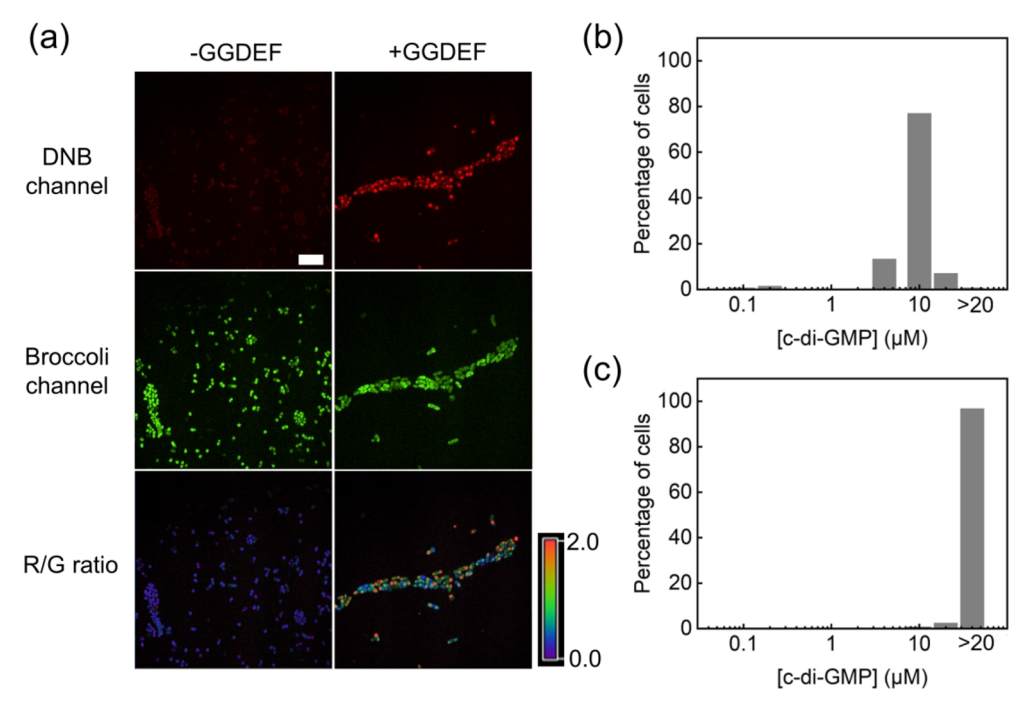


Figure 5. (a) Fluorescence imaging of c-di-GMP in live BL21 (DE3)* cells. 200 μ M DFHBI-1T and 0.5 μ M TMR-DN were added 1 h before imaging. DNB channel (red), Broccoli channel (green), and DNB-to-Broccoli (R/G) ratiometric images were shown. Scale bar, 10 μ m. (b, c) Cellular distribution of c-di-GMP in the absence (b) or presence (c) of the GGDEF domain. Individual cells were binned according to their c-di-GMP concentrations. The percentage of cells in each bin was plotted.

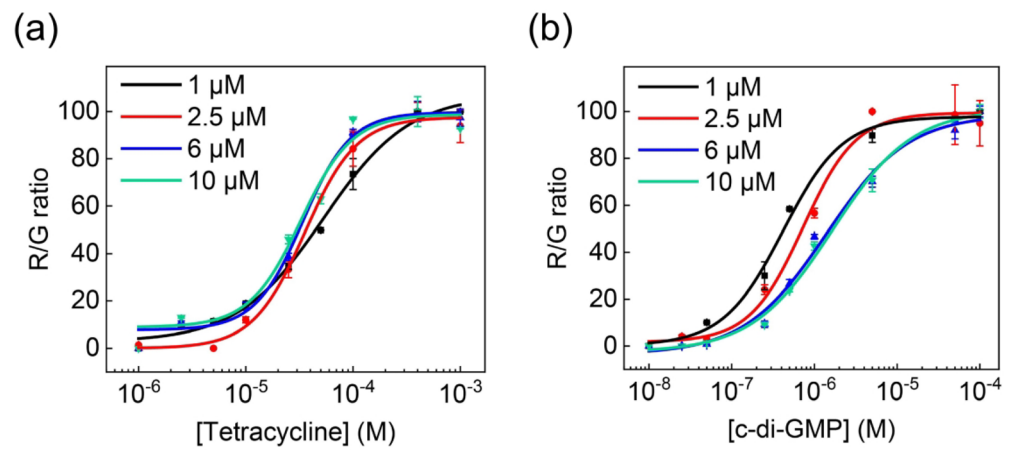


Figure 6. Dose—responsive curves for tetracycline (a) and c-di-GMP (b) were measured at varying concentrations of RNA and 0.5 μ M TMR-DN. R/G ratio indicated the fluorescence ratio as measured at $\lambda_{\rm ex}/\lambda_{\rm em}$, 555/582 nm (R) vs that at $\lambda_{\rm ex}/\lambda_{\rm em}$, 480/503 nm (G). Shown are mean and SEM values of three independent replicates.

to image and quantify target small molecules in living cells. We first cloned tetracycline-targeting F30-DNB/Broccoli sensors into BL21 (DE3)* cells. After adding 50–1000 μ M tetracycline, the cellular DNB/TMR-DN fluorescence was indeed activated in a target-dependent manner, while the Broccoli/DFHBI-1T signal was remained at a constant level (Figure 4a and b).

To further test if these RNA-based sensors could be used to detect naturally existing analytes, we prepared c-di-GMP-targeting F30-DNB/Broccoli sensors to image cellular c-di-GMP levels. To manipulate the intracellular c-di-GMP levels, we prepared BL21 (DE3)* cells expressing either a diguanylate cyclase GGDEF domain or a random sequence. The GGDEF domain was used to increase the cellular synthesis of c-di-GMP. ^{33,34} As expected, minimal DNB/TMR-DN fluorescence

was observed without the GGDEF expression (Figure 5a). In contrast, much higher DNB fluorescence was achieved in the cells expressing GGDEF. As a reference, the Broccoli fluorescence was not influenced by the GGDEF expression. DNB/Broccoli-based ratiometric sensors could be indeed used to detect signaling molecules in living cells.

Our next goal is to study if we could apply these sensors to determine the cell-to-cell variations in the target levels. We first wanted to obtain standard calibration curves for the target quantification. We prepared a series of concentrations of tetracycline-targeting F30-DNB/Broccoli sensors *in vitro* and determined their corresponding dynamic ranges for the tetracycline detection (Figure 6a). Our results indicated that independent of the RNA concentrations, the DNB-to-Broccoli fluorescence ratios were linearly correlated with \sim 10–130 μ M

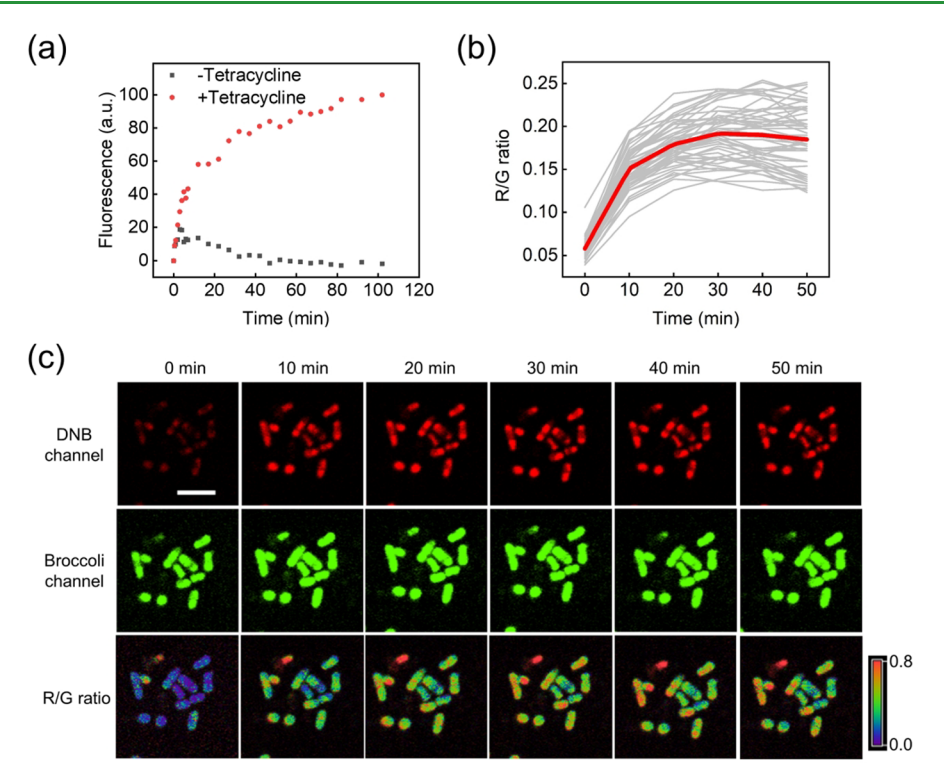


Figure 7. (a) In vitro kinetics measurement with 2.5 μM tetracycline-targeting ratiometric RNA sensor and 0.5 μM TMR-DN in the absence or presence of 500 μM tetracycline. (b) Tracking of the R/G fluorescence ratio from 55 individual cells. The fluorescence of each cell was plotted in a gray line. The averaged signal of these 55 cells was plotted in red. (c) Monitoring tetracycline accumulation dynamics in live BL21 (DE3)* cells after adding 500 μM tetracycline at 0 min. DNB sensor channel (red), Broccoli channel (green), and DNB-to-Broccoli (R/G) ratiometric images were shown. Scale bar, 5 μm.

tetracycline. Similarly, the DNB-to-Broccoli fluorescence ratios of the c-di-GMP-targeting sensors could be used to determine the c-di-GMP concentrations in the range of $\sim 0.1-20~\mu M$ (Figure 6b). The RNA concentrations we tested here (1–10 μM) are similar as those determined in living *E. coli* cells.²⁵

We next applied these ratiometric sensors to quantify target concentrations in BL21 (DE3)* cells. As shown in Figure 4a, after adding 50-1000 μ M tetracycline, we analyzed the DNBto-Broccoli fluorescence ratios of 200 individual cells at each target concentration. After subtracting the cellular background, on average a 6.2-, 8.1-, and 13.1-fold increase in the cellular DNB-to-Broccoli fluorescence ratio was observed with the addition of 250, 500, and 1000 μM tetracycline (Figure 4b). After normalizing the sensitivity differences between the fluorimeter and microscope (Figures 1c, S5b, and S6c), based on the standard calibration curves (Figure 6a), these cellular fluorescence signals were correlated with 210, 290, and 510 µM tetracycline, respectively. These determined values were consistent with that obtained from an HPLC assay²⁵ (Figure 4d). There are some differences between the determined intracellular tetracycline levels and those added in the solution. We believe it is likely due to the limited cell membrane penetration and/or the activation of membrane efflux pumps that will reduce the intracellular tetracycline concentrations. It is also worth mentioning that compared to SR-DN-based sensors,²⁵ a better signal-to-noise ratio was achieved with TMR-DN for the tetracycline imaging.

We also wondered if the cellular target concentrations could be quantified simply by only measuring the DNB fluorescence. Based on the dose-responsive curves of tetracycline-induced DNB fluorescence (Figure S7), we quantified the cellular tetracycline concentrations. However, compared to the data obtained from the ratiometric imaging, DNB-only results were obviously less consistent with the HPLC data (Figure 4d). Indeed, due to the cell-to-cell variations in the RNA expression levels, ratiometric-based quantification provided more accurate determination of target concentrations.

We further determined the cellular distributions of tetracycline. With 1 mM tetracycline added in the solution, 35%, 61%, and 4.3% of cells accumulated high (>600 μ M), medium (300–600 μ M), or low (<300 μ M) levels of tetracycline, respectively (Figure 4c). To study the correlations between the tetracycline accumulation and changes in the cell viability, we added a Sytox Blue (SB) dye to stain the dead/dying cells (Figure 4a). The percentage of SB-stained cells increased from almost zero to 38%, 48%, and 87% after 2 h incubating with 0, 100, 250, and 1000 μ M tetracycline. Among the SB-stained cells, 97% also accumulated high levels of tetracycline. Indeed, the cell viability is highly correlated with the cellular accumulations of tetracycline.

In addition to tetracycline, we also applied F30-DNB/Broccoli sensors to quantify cellular c-di-GMP concentrations. Based on the normalized fluorescence signals and standard calibration curves (Figures 6b, S5b, and S6c), the determined c-di-GMP level in cells without expressing the GGDEF domain is 8.3 μ M, which is consistent with the HPLC results, 11 μ M. While for GGDEF-expressing cells, the c-di-GMP levels were too high to be quantified (Figure Sc). There are some clear cell-to-cell variations in the c-di-GMP level. For cells that do not express the GGDEF domain, 2.1%, 90.2%, and 7.7% of cells exhibited low (<0.2 μ M), medium (0.2–10 μ M), or high (>10 μ M) levels of c-di-GMP (Figure Sb). While in contrast,

in the presence of GGDEF, 99.2% of cells exhibited high level of c-di-GMP and another 0.8% contained medium level of c-di-GMP (Figure 5c). All these results indicated that the DNB/TMR-DN and Broccoli/DFHBI-1T-based ratiometric sensors can be indeed used to image and quantify the cellular concentrations and distributions of target analytes.

Kinetic Measurement with RNA-based Ratiometric Sensors. Finally, we wanted to test if these new TMR-DN-based ratiometric sensors can be used to monitor the cellular dynamics of target analytes. Using the tetracycline-targeting F30-DNB/Broccoli sensor as an example, we first monitored the DNB/TMR-DN fluorescence signal change after mixing $500~\mu\mathrm{M}$ tetracycline with the *in vitro* transcribed RNA sensors (Figure 7a). A fast increase in the fluorescence signal was observed. It took $\sim 10~\mathrm{min}$ to reach the half-maximal fluorescence signal. As a control, the sensor fluorescence signal was quite stable in the absence of tetracycline. Indeed, we can apply TMR-DN-based RNA sensors to perform kinetic measurement.

We further applied this ratiometric sensor system to monitor the dynamic cellular accumulations of tetracycline. After mixing 500 µM tetracycline with E. coli cells that expressed the sensors, the cellular fluorescence was imaged every 10 min (Figure 7b and c). Clear cell-to-cell variations in the rates of tetracycline accumulation was observed. Under this experimental condition, 60% of cells quickly accumulated high levels of tetracycline, i.e., >200 μ M tetracycline was identified in these cells within the first 20 min. Interestingly, the tetracycline level in 10.7% of cells started to decrease after ~30 min incubation. Such decreased tetracycline levels may indicate the generation and function of membrane efflux pumps, an important mechanism for developing antibiotic resistance.³⁵ Indeed, these TMR-DN-based ratiometric sensors could be used to monitor the dynamic variations of target concentrations in living cells. Another interesting observation was that a population of these E. coli cells exhibited high levels of tetracycline either at one pole or both polar regions (Figure 7c). This may be correlated with the fact that the cellular targets of tetracycline, i.e., subunits of rRNAs, tend to accumulate at these polar regions.³⁶ Some future studies may be potentially followed to understand the detailed mechanism of these subcellular distribution patterns.

CONCLUSION

Genetically encoded fluorogenic RNA-based sensors become popular tools for the detection and imaging of cellular analytes.^{37,38} Most of these sensors are rely on a singlechannel emission for the measurement. Due to the cell-to-cell variations in the RNA expression level, it is challenging to accurately determine the cellular concentrations of target analytes based on just a single-channel fluorescence. As a result, we developed these ratiometric RNA-based sensors to accurately quantify the cellular concentrations of target analytes.²⁵ However, due to the instability of the SR-DN dye (through unknown mechanism), the previous version of the sensor failed for monitoring the dynamic changes of target cellular levels. Herein, by using a highly stable TMR-DN dye, we are able to apply the same ratiometric RNA sensor strands to monitor target levels in the living cells. To demonstrate the functions of these sensors, we chose two target analytes, tetracycline, and c-di-GMP. The successful live-cell monitoring of these targets will advance our understanding of several

biological processes, such as the mechanism of antibiotic resistance and biofilm formation.

To potentially allow these sensors for the real-time monitoring of target analytes under continuous irradiation, it is important to improve the photostability of the RNA sensors. There are several emerging fluorogenic RNA/fluorophore complexes that exhibit great photostability and brightness. ^{39–41} These complexes can emit fluorescence spanning the spectrum from cyan to red or even near-infrared region. Using a similar design principle as demonstrated in this study, these fluorogenic RNA aptamers may be potentially useful in developing ratiometric sensors, which can be applied to continuously monitor the kinetics of target analytes in living cells.

So far, including this study, almost all the fluorogenic RNA-based sensors are limited in use for prokaryotic cells. ^{11,26} An important issue that needs to be addressed is the development of expression systems that enable the accumulation of a large amount of RNA sensors inside eukaryotic cells. The recent development of circular RNA vectors could potentially allow our ratiometric sensors to quantify target analytes in eukaryotic cells. ⁴² In the future, we will test the performance of these circular RNA-based ratiometric sensors for eukaryotic imaging. With further optimization of ratiometric RNA-based sensor platform, we believe these genetically encoded sensors can be broadly applied for live-cell imaging and real-time monitoring of various metabolites, signaling molecules, and other biological compounds.

ASSOCIATED CONTENT

Supporting Information

The Supporting Information is available free of charge at https://pubs.acs.org/doi/10.1021/acsabm.9b01237.

RNA sequences used in this study, chemical structure of SR-DN, TMR-DN, scheme of fluorescence quenching of SR and TMR by DN, fluorescence stability of SR-DN, HPLC and MS characterization of TMR-DN, cellular fluorescence of F30-DNB/Broccoli, target-independent Broccoli fluorescence, fluorescence correlation between DNB/Broccoli ratio and DNB only (PDF)

AUTHOR INFORMATION

Corresponding Author

Mingxu You — Department of Chemistry, University of Massachusetts, Amherst, Massachusetts 01003, United States; orcid.org/0000-0002-5279-2340; Email: mingxuyou@umass.edu

Authors

Rigumula Wu – Department of Chemistry, University of Massachusetts, Amherst, Massachusetts 01003, United States

Aruni P.K.K. Karunanayake Mudiyanselage — Department of Chemistry, University of Massachusetts, Amherst, Massachusetts 01003, United States

Kewei Ren – Department of Chemistry, University of Massachusetts, Amherst, Massachusetts 01003, United States

Zhining Sun — Department of Chemistry, University of Massachusetts, Amherst, Massachusetts 01003, United States; orcid.org/0000-0003-0358-960X

Qian Tian – Department of Chemistry, University of Massachusetts, Amherst, Massachusetts 01003, United States Bin Zhao — Department of Chemistry, University of
Massachusetts, Amherst, Massachusetts 01003, United States
Yousef Bagheri — Department of Chemistry, University of
Massachusetts, Amherst, Massachusetts 01003, United States
David Lutati — Department of Chemistry, University of
Massachusetts, Amherst, Massachusetts 01003, United States
Puspam Keshri — Department of Chemistry, University of
Massachusetts, Amherst, Massachusetts 01003, United States

Complete contact information is available at: https://pubs.acs.org/10.1021/acsabm.9b01237

Notes

The authors declare no competing financial interest.

ACKNOWLEDGMENTS

The authors gratefully acknowledge the UMass Amherst startup grant, NIH R01AI136789, NSF CAREER, and Alfred P. Sloan Research Fellowship to M.Y. We are grateful to Dr. James Chambers for the assistance with the fluorescence imaging. The authors also thank other members in the You Lab and Dr. Craig Martin for useful discussion and valuable comments.

REFERENCES

- (1) Zhang, J.; Campbell, R. E.; Ting, A. Y.; Tsien, R. Y. Creating new fluorescent probes for cell biology. *Nat. Rev. Mol. Cell Biol.* **2002**, *3* (12), 906–918.
- (2) Okumoto, S. Imaging approach for monitoring cellular metabolites and ions using genetically encoded biosensors. *Curr. Opin. Biotechnol.* **2010**, 21 (1), 45–54.
- (3) Ni, Q.; Mehta, S.; Zhang, J. Live-cell imaging of cell signaling using genetically encoded fluorescent reporters. *FEBS J.* **2018**, 285 (2), 203–219.
- (4) Liu, D.; Evans, T.; Zhang, F. Z. Applications and advances of metabolite biosensors for metabolic engineering. *Metab. Eng.* **2015**, *31*, 35–43.
- (5) Frommer, W. B.; Davidson, M. W.; Campbell, R. E. Genetically encoded biosensors based on engineered fluorescent proteins. *Chem. Soc. Rev.* **2009**, 38 (10), 2833–2841.
- (6) Miyawaki, A.; Niino, Y. Molecular spies for bioimaging-fluorescent protein-based probes. *Mol. Cell* **2015**, 58 (4), 632–643.
- (7) Lindenburg, L.; Merkx, M. Engineering genetically encoded fret sensors. Sensors 2014, 14 (7), 11691–11713.
- (8) Germond, A.; Fujita, H.; Ichimura, T.; Watanabe, T. M. Design and development of genetically encoded fluorescent sensors to monitor intracellular chemical and physical parameters. *Biophys. Rev.* **2016**, 8 (2), 121–138.
- (9) Miyawaki, A. Development of probes for cellular functions using fluorescent proteins and fluorescence resonance energy transfer. *Annu. Rev. Biochem.* **2011**, *80*, 357–373.
- (10) Palmer, A. E.; Qin, Y.; Park, J. G.; McCombs, J. E. Design and application of genetically encoded biosensors. *Trends Biotechnol.* **2011**, 29 (3), 144–152.
- (11) Paige, J. S.; Nguyen-Duc, T.; Song, W. J.; Jaffrey, S. R. Fluorescence imaging of cellular metabolites with rna. *Science* **2012**, 335 (6073), 1194–1194.
- (12) Song, W. J.; Strack, R. L.; Jaffrey, S. R. Imaging bacterial protein expression using genetically encoded RNA sensors. *Nat. Methods* **2013**, *10*, 873–875.
- (13) You, M. X.; Litke, J. L.; Jaffrey, S. R. Imaging metabolite dynamics in living cells using a spinach-based riboswitch. *Proc. Natl. Acad. Sci. U. S. A.* **2015**, *112* (21), E2756–E2765.
- (14) Kellenberger, C. A.; Wilson, S. C.; Sales-Lee, J.; Hammond, M. C. RNA-based fluorescent biosensors for live cell imaging of second messengers cyclic di-Gmp and cyclic Amp-Gmp. *J. Am. Chem. Soc.* **2013**, *135* (13), 4906–4909.

- (15) Yu, Q. K.; Shi, J.; Mudiyanselage, A. P. K. K. K.; Wu, R.; Zhao, B.; Zhou, M.; You, M. X. Genetically encoded rna-based sensors for intracellular imaging of silver ions. *Chem. Commun.* **2019**, *55* (5), 707–710
- (16) Karunanayake Mudiyanselage, A. P.K.K.; Wu, R.; Leon-Duque, M. A.; Ren, K.; You, M. "Second-generation" fluorogenic RNA-based sensors. *Methods* **2019**, *161*, 24–34.
- (17) Filonov, G. S.; Kam, C. W.; Song, W. J.; Jaffrey, S. R. In-gel imaging of RNA processing using broccoli reveals optimal aptamer expression strategies. *Chem. Biol.* **2015**, 22 (5), 649–660.
- (18) Karunanayake Mudiyanselage, A.; Yu, Q.; Leon-Duque, M. A.; Zhao, B.; Wu, R.; You, M. Genetically encoded catalytic hairpin assembly for sensitive RNA imaging in live cells. *J. Am. Chem. Soc.* **2018**, *140* (28), 8739–8745.
- (19) Sunbul, M.; Jaschke, A. Contact-mediated quenching for RNA imaging in bacteria with a fluorophore-binding aptamer. *Angew. Chem., Int. Ed.* **2013**, 52 (50), 13401–13404.
- (20) Filonov, G. S.; Jaffrey, S. R. RNA imaging with dimeric broccoli in live bacterial and mammalian cells. *Curr. Protoc. Chem. Biol.* **2016**, 8 (1), 1–28.
- (21) Song, K. M.; Lee, S.; Ban, C. Aptamers and their biological applications. Sensors 2012, 12 (1), 612-631.
- (22) Zhou, J.; Bobbin, M. L.; Burnett, J. C.; Rossi, J. J. Current progress of RNA aptamer-based therapeutics. *Front. Genet.* **2012**, *3*, 234.
- (23) Paige, J. S.; Wu, K. Y.; Jaffrey, S. R. RNA mimics of green fluorescent protein. *Science* **2011**, 333 (6042), 642–646.
- (24) Filonov, G. S.; Moon, J. D.; Svensen, N.; Jaffrey, S. R. Broccoli: Rapid selection of an rna mimic of green fluorescent protein by fluorescence-based selection and directed evolution. *J. Am. Chem. Soc.* **2014**, 136 (46), 16299–16308.
- (25) Wu, R.; Karunanayake Mudiyanselage, A.; Shafiei, F.; Zhao, B.; Bagheri, Y.; Yu, Q.; McAuliffe, K.; Ren, K.; You, M. Genetically encoded ratiometric RNA-based sensors for quantitative imaging of small molecules in living cells. *Angew. Chem., Int. Ed.* **2019**, 58 (50), 18271–18275.
- (26) Arora, A.; Sunbul, M.; Jaschke, A. Dual-colour imaging of RNAs using quencher- and fluorophore-binding aptamers. *Nucleic Acids Res.* **2015**, 43 (21), No. gkv718.
- (27) Strack, R. L.; Song, W. J.; Jaffrey, S. R. Using spinach-based sensors for fluorescence imaging of intracellular metabolites and proteins in living bacteria. *Nat. Protoc.* **2014**, *9* (1), 146–155.
- (28) Bouhedda, F.; Autour, A.; Ryckelynck, M. Light-up RNA aptamers and their cognate fluorogens: From their development to their applications. *Int. J. Mol. Sci.* **2018**, *19* (1), No. e44.
- (29) Wittmann, A.; Suess, B. Selection of tetracycline inducible self-cleaving ribozymes as synthetic devices for gene regulation in yeast. *Mol. BioSyst.* **2011**, *7* (8), 2419–2427.
- (30) Wang, X. C.; Wilson, S. C.; Hammond, M. C. Next-generation RNA-based fluorescent biosensors enable anaerobic detection of cyclic di-gmp. *Nucleic Acids Res.* **2016**, 44 (17), No. e139.
- (31) Kalia, D.; Merey, G.; Nakayama, S.; Zheng, Y.; Zhou, J.; Luo, Y.; Guo, M.; Roembke, B. T.; Sintim, H. O. Nucleotide, c-di-Gmp, c-di-Amp, cGmp, cAmp, (p)ppGpp signaling in bacteria and implications in pathogenesis. *Chem. Soc. Rev.* **2013**, 42 (1), 305–41.
- (32) Chang, C. F.; Chang, L. C.; Chang, Y. F.; Chen, M.; Chiang, T. S. Antimicrobial susceptibility of actinobacillus pleuropneumoniae, escherichia coli, and salmonella choleraesuis recovered from taiwanese swine. *J. Vet. Diagn. Invest.* **2002**, *14* (2), 153–157.
- (33) Simm, R.; Morr, M.; Kader, A.; Nimtz, M.; Romling, U. Ggdef and eal domains inversely regulate cyclic di-Gmp levels and transition from sessility to motility. *Mol. Microbiol.* **2004**, *53* (4), 1123–1134.
- (34) Seshasayee, A. S. N.; Fraser, G. M.; Luscombe, N. M. Comparative genomics of cyclic-di-Gmp signalling in bacteria: Post-translational regulation and catalytic activity. *Nucleic Acids Res.* **2010**, 38 (18), 5970–5981.
- (35) Webber, M. A.; Piddock, L. J. V. The importance of efflux pumps in bacterial antibiotic resistance. *J. Antimicrob. Chemother.* **2003**, *51* (1), 9–11.

- (36) Chai, Q.; Singh, B.; Peisker, K.; Metzendorf, N.; Ge, X. L.; Dasgupta, S.; Sanyal, S. Organization of ribosomes and nucleoids in escherichia coli cells during growth and in quiescence. *J. Biol. Chem.* **2014**, 289 (16), 11342–11352.
- (37) Sun, Z. N.; Nguyen, T.; McAuliffe, K.; You, M. X. Intracellular imaging with genetically encoded RNA-based molecular sensors. *Nanomaterials* **2019**, *9* (2), No. E233.
- (38) You, M.; Litke, J. L.; Wu, R.; Jaffrey, S. R. Detection of low-abundance metabolites in live cells using an RNA integrator. *Cell Chem. Biol.* **2019**, 26 (4), 471–481.
- (39) Wirth, R.; Gao, P.; Nienhaus, G. U.; Sunbul, M.; Jaschke, A. Sira: A silicon rhodamine-binding aptamer for live-cell superresolution RNA imaging. *J. Am. Chem. Soc.* **2019**, *141* (18), 7562–7571.
- (40) Bouhedda, F.; Fam, K. T.; Collot, M.; Autour, A.; Marzi, S.; Klymchenko, A.; Ryckelynck, M. A dimerization-based fluorogenic dye-aptamer module for RNA imaging in live cells. *Nat. Chem. Biol.* **2020**, *16* (1), 69–76.
- (41) Chen, X.; Zhang, D.; Su, N.; Bao, B.; Xie, X.; Zuo, F.; Yang, L.; Wang, H.; Jiang, L.; Lin, Q.; Fang, M.; Li, N.; Hua, X.; Chen, Z.; Bao, C.; Xu, J.; Du, W.; Zhang, L.; Zhao, Y.; Zhu, L.; Loscalzo, J.; Yang, Y. Visualizing RNA dynamics in live cells with bright and stable fluorescent rnas. *Nat. Biotechnol.* **2019**, *37* (11), 1287–1293.
- (42) Litke, J. L.; Jaffrey, S. R. Highly efficient expression of circular RNA aptamers in cells using autocatalytic transcripts. *Nat. Biotechnol.* **2019**, *37*, 667–675.